

Experimental Comparison of Multiple RIS-Enabled Self-Localization Techniques Using FMCW Radar

Marc Subirà Pons, José A. López-Salcedo, Gonzalo Seco-Granados
 Marc.Subira@autonoma.cat, Jose.Salcedo@uab.cat, Gonzalo.Seco@uab.cat
 IEEC-CERES, Universitat Autònoma de Barcelona (UAB), Spain.

Abstract—This paper presents an experimental comparison of multiple Reconfigurable Intelligent Surface (RIS)-enabled self-localization techniques using Frequency-Modulated Continuous Wave (FMCW) radar. The localization techniques leverage Angle-of-Departure (AoD) and distance estimates from each RIS to enable precise localization of a User Equipment (UE). A dedicated millimeter-wave band demonstrator, incorporating a TI FMCW radar as the UE and a Sivers multiantenna transceiver to emulate RIS functionality, is used to validate the proposed techniques. The results demonstrate the feasibility of self-localization using a limited number of RIS in a linear deployment. Additionally, the robustness of AoD-based and distance difference-based methods against unknown bias errors, introduced due to the physical limitations of the demonstrator, is highlighted. This work identifies the potential of RIS-enabled self-localization in future 6G wireless communication systems, offering insights into the trade-offs between system complexity and localization accuracy in scenarios where no base station is utilized.

I. INTRODUCTION

Reconfigurable Intelligent Surfaces (RIS) have emerged as a promising technology for 6G wireless systems, enabling programmable control of electromagnetic wave reflections. Furthermore, research and experimentation on leveraging the future deployment of RIS worldwide to enable or assist User Equipment (UE) localization have gained increasing attention [1].

In context of self-localization, a single RIS reflects UE-emitted signals across its full forward-facing angular coverage. Then, the UE can process the received signals to determine its relative direction with respect to the RIS in Line of Sight (LoS) conditions. In the other hand, Frequency-Modulated Continuous Wave (FMCW) radar is widely used for high-precision distance and velocity estimation. FMCW radar transmits chirp signals and estimates distances by measuring the propagation delay through the frequency of the reflected signals [2].

Multi-RIS configurations enable flexible UE localization through different measurement approaches, using only Angle-of-Departure (AoD), only Round-Time-Trip (RTT), or combining both. This provides adaptability to various environments and measurement conditions. By optimally fusing measurements across multiple RISs, the proposed approach achieves enhanced performance compared to single-RIS solutions, leveraging the benefits of measurement redundancy.

This activity has been partially supported by the Catalan Government in the framework of the NewSpace Strategy of Catalonia, Grant PID2023-152820OB-I00 funded by MICIU/AEI/10.13039/501100011033 and by ERDF/EU, Grant PDC2023-145858-I00 funded by MICIU/AEI/10.13039/501100011033 and by the European Union NextGenerationEU/PRTR, and the AGAUR - ICREA Academia Program.

Bulding on prior work in RIS-enabled self-localization using FMCW radar [2] and multiple RIS-assisted positioning [3] we presents a comparative analysis of RIS-enabled self-localization methods using experimental data from a real demonstrator. Our testbed implements a Texas Instruments (TI) FMCW radar as the UE and emulates RIS functionality using a Sivers Semiconductors phased antenna array.

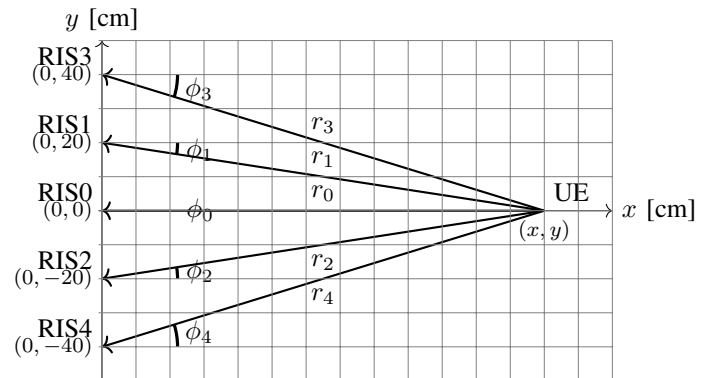


Fig. 1. Setup scheme for multiple RIS-assisted localization. The UE is located at an unknown position (x, y) , and multiple RIS are positioned along the y -axis. The distances between the UE and each RIS are denoted as r_0, r_1, r_2, r_3 , and r_4 , while the angles of the lines connecting the UE to the RIS elements with respect to the x -axis are labeled as $\phi_0, \phi_1, \phi_2, \phi_3$, and ϕ_4 .

II. MULTIPLE RIS-ENABLED SELF-LOCALIZATION

FMCW radars are capable of creating a map of stationary objects in the environment by continuously scanning the surroundings and averaging the radar range profiles over time [2]. This map enables distinguishing between static environmental features and dynamic objects or actively reflected signals aimed with a RIS, even in densely cluttered scenarios. Our framework exploits this capability to enable robust RIS-aided localization.

A. Angle of departure estimation

AoD estimation is critical for accurate RIS-assisted localization. We implement a beam-based AoD algorithm [2], [3] through two key steps

- **Beam-Sweep Acquisition**

- The FMCW radar transmits chirps while the RIS systematically sweeps all azimuth angles.
- For each angle, M chirps are averaged to suppress noise in the range profiles.

- **Clutter Rejection**

- Static environmental reflections and clutter are mitigated by subtracting the average range profile,

computed by averaging the range profiles across all azimuth angles.

- The AoD is estimated as the residual range profile with higher total energy.

Thus, the AoD estimate ϕ_i for the i -th RIS, where $i = 1, \dots, N$, is given by

$$\hat{\phi}_i = \arg \max_{\phi} \int_0^{\Delta} [P_{i,\phi}(r) - M_i(r)] dr \quad (1)$$

$$M_i(r) = \frac{1}{K} \sum_{k=0}^K P_{i,\phi_k}(r) \quad (2)$$

where $P_{i,\phi}(r)$ represents the averaged (over M chirps) range profile when its steering angle is ϕ , $M_i(r)$ is the average of the $P_{i,\phi}(r)$ over all used values of ϕ , K is the total number of steering angles and Δ is the maximum distance acceptable for our demonstrator.

B. Distance estimation

The distance r_i between the UE radar and the i -th RIS determination is achieved by analyzing the clutter-corrected range profile at the estimated AoD ϕ_i . The peak detection of this profile yields the distance measurement

$$\hat{r}_i = \arg \max_r [P_{i,\hat{\phi}_i}(r) - M_i(r)] \quad (3)$$

C. Localization estimation

Given AoD and distance estimates for each RIS, the UE location $\mathbf{p} = [x, y]^T$ can be estimated using various methods, depending on the specific measurements. In this work, we assume a linear RIS deployment, where all RIS elements are positioned along the y -axis. Thus, the i -th RIS is located at $\mathbf{a}_i = [x_i, y_i]^T = [0, y_i]^T$. This kind of setup could be viable, for example, in indoor applications (where the RIS is deployed on the same wall).

The distance difference d_i between RIS i and RIS 0 and its estimate \hat{d}_i are given by

$$d_i = \|\mathbf{p} - \mathbf{a}_i\| - \|\mathbf{p} - \mathbf{a}_0\|, \quad (4)$$

$$\hat{d}_i = \hat{r}_i - \hat{r}_0 \quad (5)$$

1) *Single RIS self-localization*: Given AoD and distance estimates from a single RIS, the UE position can be estimated by combining both measurements

$$\hat{\mathbf{p}} = \begin{pmatrix} \hat{x} \\ \hat{y} \end{pmatrix} = \begin{pmatrix} x_0 + \hat{r}_0 \cos(\hat{\phi}_0) \\ y_0 + \hat{r}_0 \sin(\hat{\phi}_0) \end{pmatrix} \quad (6)$$

2) *Self-localization with distances*: This approach leverages only distance measurements obtained from multiple RISs. By employing the principle of intersecting multiple circles, the UE position can be determined without requiring any angle measurements. While the general case for arbitrary RIS deployments is covered in [4, Chapter 7], our linear deployment along the y -axis requires special consideration.

The problem begins with the Euclidean distance relationships between the UE and each RIS. Simplifying these equations exploits the geometric constraint that all RISs share the same x -coordinate ($x_i = 0$), reducing the system to

depend only on y . Subtracting two equations from different RISs yields a linear system in y :

$$r_i^2 = (y - y_i)^2 + x^2 \quad (7)$$

$$r_i^2 - r_0^2 = -2y(y_i - y_0) + y_i^2 + y_0^2 \quad (8)$$

To solve for the y -coordinate, we rearrange the linearized system in matrix form

$$\underbrace{\begin{pmatrix} y_1 - y_0 \\ y_2 - y_0 \\ \vdots \\ y_{N-1} - y_0 \end{pmatrix}}_{\mathbf{h}} y = \underbrace{\begin{pmatrix} \frac{(y_1^2 - r_1^2) - (y_0^2 - r_0^2)}{2} \\ \frac{(y_2^2 - r_2^2) - (y_0^2 - r_0^2)}{2} \\ \vdots \\ \frac{(y_{N-1}^2 - r_{N-1}^2) - (y_0^2 - r_0^2)}{2} \end{pmatrix}}_{\mathbf{b}} \quad (9)$$

where \mathbf{h} and \mathbf{b} are constructed from RIS positions and distance measurements.

The least-squares (LS) estimate \hat{y} is given by

$$\hat{y} = (\mathbf{h}^T \mathbf{h})^{-1} \mathbf{h}^T \mathbf{b} \quad (10)$$

Using \hat{y} , the x -coordinate is derived from the distance constraints

$$x = \sqrt{r_i^2 - (y_i - \hat{y})^2} = \sqrt{r_i^2 - (y_i - \hat{y})^2} \quad (11)$$

Each RIS contributes a candidate x -value, forming an overdetermined system

$$\mathbf{1} \cdot x = \underbrace{\begin{pmatrix} \sqrt{r_1^2 - (y_1 - \hat{y})^2} \\ \sqrt{r_2^2 - (y_2 - \hat{y})^2} \\ \vdots \\ \sqrt{r_{N-1}^2 - (y_{N-1} - \hat{y})^2} \end{pmatrix}}_{\tilde{\mathbf{b}}} \quad (12)$$

The LS solution simplifies to the arithmetic mean of the candidate values

$$\hat{x} = (\mathbf{1}^T \mathbf{1})^{-1} \mathbf{1}^T \tilde{\mathbf{b}} = \frac{\mathbf{1}^T \tilde{\mathbf{b}}}{N} \quad (13)$$

where $\mathbf{1}$ represents a vector of ones.

3) *Self-localization with Distance Differences*: This method is based on hyperbolic positioning [5] that utilizes distance differences. In this case, our linear RIS deployment along the y -axis again permits a simplified closed-form solution.

The derivation begins with the hyperbolic distance-difference equation. Expanding and simplifying these equations cancel common quadratic terms, resulting in a linear relationship that couples the UE y -coordinate with the 0-th RIS distance $r_0 = \|\mathbf{p} - \mathbf{a}_0\|$ as shown below:

$$(d_i - \|\mathbf{p} - \mathbf{a}_0\|)^2 = \|\mathbf{p} - \mathbf{a}_i\|^2 \quad (14)$$

$$d_i^2 + \|\mathbf{p} - \mathbf{a}_0\|^2 - 2d_i \|\mathbf{p} - \mathbf{a}_0\| = \|\mathbf{p} - \mathbf{a}_i\|^2 \quad (15)$$

$$y(y_i - y_0) - d_i r_0 = \frac{\|a_i\|^2 - \|a_0\|^2 - d_i^2}{2} \quad (16)$$

Similar to the distance-base approach, the system is reformulated in matrix notation

$$\underbrace{\begin{pmatrix} -d_1 & y_1 - y_0 \\ -d_2 & y_2 - y_0 \\ \vdots & \vdots \\ -d_{N-1} & y_{N-1} - y_0 \end{pmatrix}}_{\mathbf{H}_d} \begin{pmatrix} r_0 \\ y \end{pmatrix} = \underbrace{\begin{pmatrix} \frac{\|\mathbf{a}_1\|^2 - \|\mathbf{a}_0\|^2 - d_1^2}{2} \\ \frac{\|\mathbf{a}_2\|^2 - \|\mathbf{a}_0\|^2 - d_2^2}{2} \\ \vdots \\ \frac{\|\mathbf{a}_{N-1}\|^2 - \|\mathbf{a}_0\|^2 - d_{N-1}^2}{2} \end{pmatrix}}_{\mathbf{b}_d} \quad (17)$$

where \mathbf{H} and \mathbf{b} now incorporate distance difference measurements instead of distance measurements.

The system is solved using weighted least squares (WLS) since there are a correlation in the measurements

$$\begin{pmatrix} \hat{r}_0 \\ \hat{y} \end{pmatrix} = (\mathbf{H}_d^T \mathbf{W}^{-1} \mathbf{H}_d)^{-1} \mathbf{H}_d^T \mathbf{W}^{-1} \mathbf{b}_d \quad (18)$$

Here, the weight matrix \mathbf{W} is formulated as

$$\mathbf{W} = \sigma_d^2 (\mathbf{I} + \mathbf{1} \mathbf{1}^T), \quad (19)$$

in which \mathbf{I} denotes the identity matrix, and σ_d^2 is the noise variance associated with the distance measurements.

Finally, \hat{x} is computed from the distance constraint between the UE and the reference RIS

$$\hat{x} = \sqrt{\hat{r}_0^2 - y_0^2 - \hat{y}^2} + x_0. \quad (20)$$

4) *Self-localization with angles*: This technique applies the principle of triangulation based on AoD measurements from multiple RISs to estimate the UE position [6, Chapter 4]. Unlike prior methods requiring distance or difference in distance data, this approach relies solely on angular measurements.

The formulation begins with the geometric relationship between the UE position \mathbf{p} , the i -th RIS location, and the AoD ϕ_i under LoS conditions, following the subsequent relationship

$$y - y_i = \tan(\phi_i) (x - x_i) \quad (21)$$

$$(\tan(\phi_i) \quad 1) \mathbf{p} = y_i - \tan(\phi_i) x_i \quad (22)$$

In this case, rearranging into matrix form enables the estimation of the entire UE location \mathbf{p} at once

$$\underbrace{\begin{pmatrix} -\tan(\hat{\phi}_0) & 1 \\ -\tan(\hat{\phi}_1) & 1 \\ \vdots & \vdots \\ -\tan(\hat{\phi}_{N-1}) & 1 \end{pmatrix}}_{\mathbf{H}_a} \mathbf{p} = \underbrace{\begin{pmatrix} y_0 - \tan(\hat{\phi}_0)x_0 \\ y_1 - \tan(\hat{\phi}_1)x_1 \\ \vdots \\ y_{N-1} - \tan(\hat{\phi}_{N-1})x_{N-1} \end{pmatrix}}_{\mathbf{b}_a}. \quad (23)$$

we then estimate the UE location \mathbf{p} using LS.

5) *Self-localization with distance differences and angles*: In this advanced method, we aim to join distance differences and angles techniques. This method relies on both distance differences and AoD measurements from all RIS elements are combined to enhance localization accuracy.

By joining system of equations presented in Equations (17) and (23) we get a system depending on r_0 , y and x .

The new matrix \mathbf{H}_{da} is computed in Matlab notation as

$$\mathbf{H}_{da} = \begin{pmatrix} \mathbf{H}_d(:, 1) & \mathbf{0} & \mathbf{H}_d(:, 2) \\ \mathbf{0} & \mathbf{H}_a(:, 1) & \mathbf{H}_a(:, 2) \end{pmatrix} \quad (24)$$

and vector \mathbf{b}_{da} is the concatenation of \mathbf{b}_d and \mathbf{b}_a .

We apply LS to resolve the total system resulting in

$$\begin{pmatrix} \hat{r}_0 \\ \hat{x} \\ \hat{y} \end{pmatrix} = (\mathbf{H}_{da}^T \mathbf{W}_{da}^{-1} \mathbf{H}_{da})^{-1} \mathbf{H}_{da}^T \mathbf{W}_{da}^{-1} \mathbf{b}_{da} \quad (25)$$

where \mathbf{W}_{dd-a} is computed as

$$\mathbf{W}_{dda} = \begin{pmatrix} \mathbf{W} & \mathbf{0} \\ \mathbf{0} & \sigma_a^2 \mathbf{I} \end{pmatrix} \quad (26)$$

where σ_a^2 is the noise variance associated with the AoD measurements.

Lastly, x is estimated as the average of \hat{x} obtained from Equation (25) and the result of applying the new values of \hat{r}_0 and \hat{y} to Equation (20).

III. EXPERIMENTAL SETUP AND RESULTS

To validate the proposed multiple RIS-enabled self-localization system, we conducted experimental evaluations using the setup illustrated in Figure 1.

The main hardware components are

- **FMCW Radar as UE**: The system employs the TI AWR6843ISK mmWave radar [7], which operates in the frequency range of 60 GHz to 64 GHz. This radar utilizes its onboard processing capabilities to compute the radar range profile with 3.9 cm resolution, enabling real-time detection and ranging of objects in its field of view.
- **RIS Emulator**: RIS functionality is implemented using the Sivers Semiconductors EVK06002 evaluation kit [8], which integrates the RF Module BFM06010. This emulator supports beamsteering within an azimuth range of -45° to $+45^\circ$ with a approximated steering precision of -1.5° . It can retransmit received signals by connecting its RX outputs to its TX inputs, effectively replicating the behavior of a passive RIS.

The FMCW signal used is a chirp with a sawtooth modulation pattern. The initial frequency is 60 GHz, with a frequency slope of 20MHz/ μ s and a ramp duration of 200 μ s, resulting in a total bandwidth of 4 GHz. The received down-chirped signal is sampled using an ADC with a sampling frequency of 2 MHz. However, due to system stabilization constraints, only the central 384 samples are retained, instead of the full 400 samples. Additionally, the received signal is filtered using a high-pass filter with a cutoff frequency of 175 kHz.

We used $N = 5$ total RISs as depicted in Figure 1 and $M = 20$ chirps captures average for each range profile.

Figure 2 illustrates the process of clutter rejection from the radar range profiles. The first plot overlays all radar range profiles acquired for each angle of arrival of a single RIS, each represented by a different color. The second plot shows the difference between the radar range profiles and the stationary object map, which is computed by averaging all radar range profiles. It can be observed that while some angles exhibit significant variation due to the received signal, others show only minor variations, likely caused by noise.

Figure 3 illustrates the continuation of the estimation process. The first plot represents the total integrated power variation obtained for each angle. The angle of departure (AoD) estimate is then computed by identifying the angle corresponding to the maximum total variation, as described in Equation (1). Finally, the distance estimation is derived using

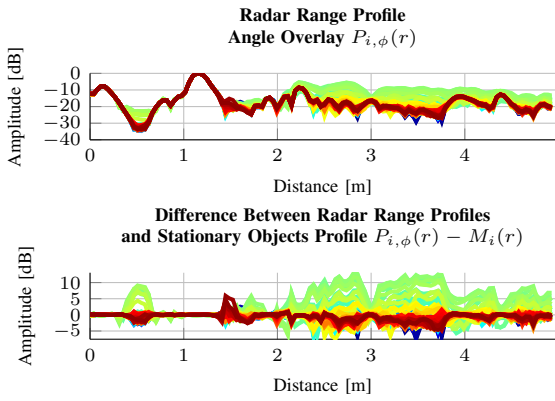


Fig. 2. Example of Clutter Rejection Process.

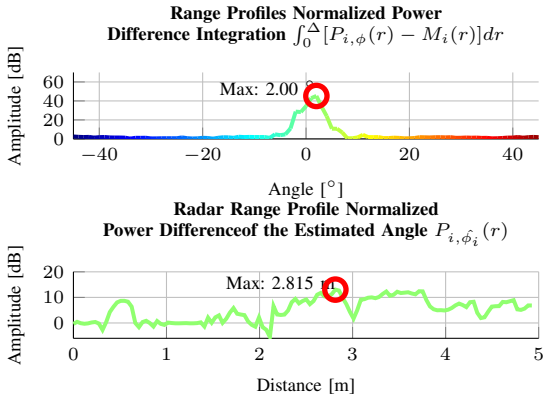


Fig. 3. Example of AoD and Range Estimation Process.

Equation (3). In this case, the results indicate a deviation of 2° in the angle estimation and a distance estimation error of 2.015 m.

The total measured error is caused by multiple factors, such as noise and multipath propagation. However, the most significant contributor is the delay introduced by the emulator, which has been estimated through multiple tests to correspond to approximately 2 m.

The results validate the effectiveness of localization using multiple RIS elements, demonstrating a significant enhancement over methods relying on a single RIS, as illustrated in Figure 4.

IV. CONCLUSIONS

In this paper, we have presented a comprehensive analysis of multiple RIS-enabled self-localization techniques utilizing FMCW radar. We proposed simple yet effective methods for AoD and distance estimation, along with a variety of localization approaches, including single RIS-based localization, distance-based localization, distance difference-based localization, AoD-based localization, and a hybrid approach combining AoD and distance measurements.

Our study revealed that distance-based methods are susceptible to unknown bias errors, which can substantially degrade performance. In contrast, distance difference-based methods are immune to such errors but yield less accurate results when bias error is known. The AoD-based method outperformed

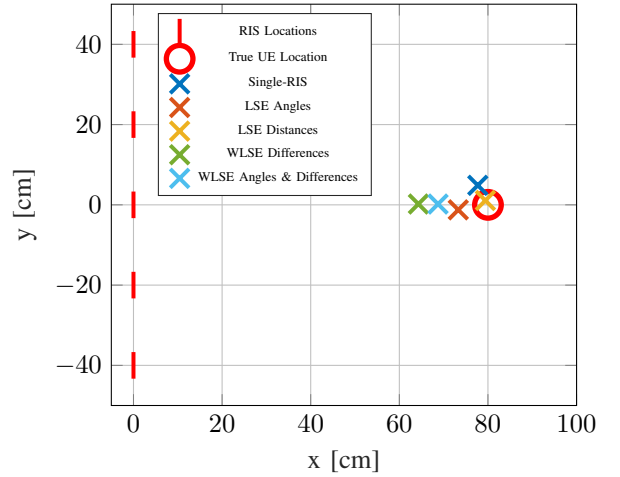


Fig. 4. UE position estimates obtained with different methods.

the distance difference-based approach but required precise synchronization with the RIS devices.

The findings highlight the promising potential of RIS-enabled self-localization for future 6G wireless communication systems, particularly in scenarios where traditional base station infrastructure or GNSS systems are unavailable or impractical.

Building on these results, we will focus on improving the accuracy of distance and AoD estimation, particularly at extended ranges, and integrating advanced signal processing techniques, to further enhance localization performance. Additionally, we will conduct extensive field testing and simulations to evaluate the system's performance under real-world conditions.

REFERENCES

- [1] H. Wymeersch, J. He, B. Denis, A. Clemente, and M. Juntti, "Radio Localization and Mapping with Reconfigurable Intelligent Surfaces: Challenges, Opportunities, and Research Directions," *IEEE Vehicular Technology Magazine*, 2020.
- [2] H. Kim, N. Amani, M. F. Keskin, *et al.*, "RIS-Enabled Self-Localization with FMCW radar," *Submitted*, 2025.
- [3] K. Keykhosravi, B. Denis, G. C. Alexandropoulos, *et al.*, "Leveraging RIS-Enabled Smart Signal Propagation for Solving Infeasible Localization Problems: Scenarios, Key Research Directions, and Open Challenges," *IEEE Vehicular Technology Magazine*, 2023.
- [4] A. Bensusky, *Wireless Positioning Technologies and Applications, Second Edition*. 2008, vol. 1.
- [5] Y. Chan and K. Ho, "A Simple and Efficient Estimator for Hyperbolic Location," *IEEE Transactions on Signal Processing*, 1994.
- [6] S. Sand, C. Mensing, and A. Dammann, *Positioning in Wireless Communications Systems – Introduction and Overview*. 2014.
- [7] T. Instruments. (2025), [Online]. Available: <https://www.ti.com/tool/AWR6843ISK>.
- [8] Sivers. (2025), [Online]. Available: <https://www.sivers-semiconductors.com/5g-millimeter-wave-mmwave-and-satcom/wireless-products/evaluation-kits/evaluation-kit-evk06002/>.